Astron. Astrophys. 283, 247–262 (1994)

ASTRONOMY AND ASTROPHYSICS

Seismic study of overshoot at the base of the solar convective envelope

M.J.P.F.G. Monteiro[1,2], J. Christensen-Dalsgaard[3], and M.J. Thompson[1]

[1] Astronomy Unit, School of Mathematical Sciences, Queen Mary & Westfield College, Mile End Rd., London E1 4NS, England
[2] Grupo de Matemática Aplicada da Faculdade de Ciências, and Centro de Astrofísica, Universidade do Porto, Porto, Portugal
[3] Institut for Fysik og Astronomi, Aarhus Universitet, DK-8000 Aarhus C, Denmark

Received 7 July 1993 / Accepted 16 August 1993

Abstract. Sharp transitions in the internal stratification of a star give rise to a characteristic signature in normal-mode frequencies. In particular, if in the Sun such a feature were located well inside the acoustic cavity of many solar p modes, it would give rise to a signal that was a periodic function of the frequency of the modes. We use this signature to detect the base of the solar convection zone and to investigate the existence of convective overshoot into the radiative interior. Two methods are considered. The "absolute" method obtains the residuals in the frequencies after making a smooth fit in mode order n, and then uses an asymptotic description of the eigenfunctions to make a fit to the residuals. The "differential" method makes an asymptotic fit to the differences between solar frequencies and the frequencies of a theoretical model. Various theoretical models of overshoot at the base of the convection zone predict the existence of a rather abrupt transition to subadiabatic stratification at the base of the overshoot region. We find no strong evidence for the existence of an overshoot region of this kind. Indeed if the overshoot consists of an essentially adiabatic extension of the convection zone followed by an abrupt transition to radiative stratification then we may (at the 95% confidence level) put an upper limit of 0.07 local pressure scale heights on the extent of the overshoot layer.

Key words: Sun: interior – Sun: oscillations – convection

1. Introduction

The Sun oscillates in modes which correspond to waves trapped between the surface layers and a lower region in which the waves undergo total internal reflection. Each mode has an associated resonant cavity defined by these two reflecting boundaries, and therefore the characteristics of a mode, e.g. its frequency, will depend on the properties of the medium constituting the cavity. By using such a dependence, helioseismology has proved to be an excellent window on the interior of the Sun, providing otherwise inaccessible information about the physics of the solar interior.

From our ignorance of the physics of convection comes one of the present problems in stellar structure: to investigate the existence and extent of convective overshoot under stellar conditions and its effects on the equilibrium configuration and evolution of a star. An overshoot layer in the Sun is generally expected at the boundary between the convectively stable radiative interior and the envelope where the fluid undergoes convective motions. Indeed, hydrodynamic simulations, and the observation of other transition layers in nature, suggest that convective motions within the gas do tend to penetrate beyond the convectively unstable region into the region in radiative equilibrium, therefore forcing a configuration where the near-adiabatic stratification goes below the boundary location predicted by the Schwarzschild stability condition. When modelling stars, overshoot from a convective envelope should be included (e.g. Alongi et al. 1991). Even more significant is the similar process of overshoot from a convective core; this would add fuel to the nuclear-burning region of the star and hence would strongly affect the evolution of the star (e.g. Maeder 1976). But since we have no reliable theory to predict the penetration depth as a function of the local stratification, the effect is in general modelled through the introduction of a parameter (similar to the ratio α between mixing length and pressure scale height employed in mixing-length theory). Such a parametric description must be constrained observationally if any predictive capability is to be retained from modelling stellar interiors.

The work presented here is an attempt to determine, using solar seismic data, whether overshoot is present at the base of the solar convective envelope and to put an upper limit on its extent. The basic idea is that any abrupt change in the stratification of the star, such as occurs in the local sound speed at the base of the convection zone, will contribute with a characteristic periodic signal to the frequencies of oscillation. Thus, if such a periodic signal can be isolated and analyzed, the relation between the local conditions and the characteristics of the signal may be used to infer valuable information concerning that region. In particular, the period is associated with the acoustic depth of such a feature in the structure (e.g. Gough 1990), while the amplitude of the

signal is related to the abruptness of the transition. If the transition from adiabatic to subadiabatic stratification occurs where the Schwarzschild condition is marginally satisfied the second derivative of the sound speed is discontinuous. However, several theoretical models (e.g. Schmitt et al. 1984; Zahn 1991) suggest that in the presence of overshoot it is the first derivative that is discontinuous. Therefore, one expects to see a much higher amplitude of the periodic signal in the seismic data if overshoot is present, the amplitude increasing as the penetration depth of the overshooting gas increases.

Pursuing this possibility we construct a method for isolating this signal in the frequencies and through the study of its characteristics provide a direct constraint on the penetration distance at the base of the convective envelope in the Sun. Briefly, our method consists of an iterative process whereby a smoothing function is used to remove a 'smooth' approximation to the frequencies of oscillation, leaving in the residuals the periodic signal we are trying to study. We then fit to the residuals, considered as a function of mode frequency, an asymptotic expression obtained from a variational principle for nonradial oscillations. Major complications in such an isolation procedure are the relatively small amplitude signal we are dealing with, and the contribution to the frequencies from other localized effects, such as the helium ionization zone.

We start by deriving an asymptotic expression for the signature in the frequencies of oscillation of the transition layer at the base of the solar convective envelope, using a variational principle for adiabatic nonradial oscillations. A simple analogy is presented to elucidate the underlying physical reason for this signature and its periodicity. If moderate-degree data are included the simple relation of the periodic signal with period given by the acoustic depth of the transition layer is destroyed. Hence we introduce a compensating higher-order term to allow the use of such moderate-degree data. A discussion of the contribution from the surface layers is also presented in order to estimate the effect on the values inferred for the parameters of the signal. After describing the numerical method used to isolate the signal, the models constructed to test the method are presented and the results reported. Finally, we present a complementary method which uses frequency differences between the Sun and a theoretical model. The possibilities of using this method are briefly discussed. The paper ends with a discussion of the implications of our results for overshoot at the base of the solar convective envelope.

2. Variational analysis

We consider a variational principle for nonradial adiabatic oscillations, assuming zero pressure at the surface located at radius R as a boundary condition (Chandrasekhar 1964; Unno et al. 1979). For high-order acoustic modes one may neglect terms associated with the perturbation in the gravitational potential, to obtain

$$\omega^2 = I_2/I_1 \,, \tag{1}$$

where

$$I_1 = \int_0^R r^2 \rho(\xi_r^2 + L^2\xi_h^2)\mathrm{d}r \tag{2}$$

and

$$I_2 = \int_0^R r^2\rho\left\{\frac{c^2}{r^4}\left[\frac{\mathrm{d}(r^2\xi_r)}{\mathrm{d}r}\right]^2 - \frac{g}{\rho}\frac{\mathrm{d}\rho}{\mathrm{d}r}\xi_r^2 + S_l^2L^2\xi_h^2 - \right.$$
$$\left. - \frac{g}{r^4}\frac{\mathrm{d}(r^4\xi_r^2)}{\mathrm{d}r} - \frac{2S_l^2}{r}\xi_h\frac{\mathrm{d}(r^2\xi_r)}{\mathrm{d}r} + \frac{2g}{r}\xi_rL^2\xi_h\right\}\mathrm{d}r \,. \tag{3}$$

Here ω is the frequency of the mode, and r, ρ, c and g are distance from the centre, density, adiabatic sound speed and gravitational acceleration, respectively. The Lamb frequency is $S_l = Lc/r$ with $L^2 = l(l+1)$, l being the degree of the mode, and the horizontal and vertical components of the displacement vector are, respectively, ξ_h and ξ_r.

In a simple analysis of the overshoot region the transition from adiabatic stratification, extended due to the penetration of the convective motions, to radiative energy transport can be regarded as discontinuous (Pidatella & Stix 1986; Zahn 1991). This implies that instead of having a discontinuous second derivative of the sound speed due to the transition from convectively unstable to stable regions we have a discontinuity in the first derivative resulting from the forced adiabatic stratification into the stable region. Such features may be regarded as localized perturbations to a smooth structure, the condition for smoothness being that the scale height of the second derivative of the sound speed be much larger than the local wavelength of the modes. The actual star differs from the smooth model by having small localized deviations $\delta\rho$ and δc^2 in its structure, resulting from smoothing the discontinuity at the base of the convective envelope.

We now apply the variational principle to obtain the change in frequency, due to the small perturbations $\delta\rho$ and δc^2, from the value ω_0 for the smooth reference model. The result is

$$\delta\omega^2 = \omega^2 - \omega_0^2 = \frac{\delta I_2 - \omega_0^2\delta I_1}{I_1} = \frac{\delta I}{I_1} \,, \tag{4}$$

where

$$\delta I = \int_0^R \left\{ - r^2 g\xi_r^2\frac{\mathrm{d}\delta\rho}{\mathrm{d}r} + \frac{1}{r^2}\left[\frac{\mathrm{d}(r^2\xi_r)}{\mathrm{d}r}\right]^2\delta(\rho c^2) + L^4\xi_r^2\,\delta(\rho c^2) - \right.$$
$$- \frac{2}{r}L^2\xi_h\frac{\mathrm{d}(r^2\xi_r)}{\mathrm{d}r}\delta(\rho c^2) - \frac{g}{r^2}\frac{\mathrm{d}(r^4\xi_r^2)}{\mathrm{d}r}\delta\rho +$$
$$\left. + 2rg\,\xi_rL^2\xi_h\,\delta\rho - \omega_0^2r^2(\xi_r^2 + L^2\xi_h^2)\,\delta\rho\right\}\mathrm{d}r \,. \tag{5}$$

All quantities correspond now to the equilibrium structure of the smooth star.

By integrating by parts, and neglecting the perturbation to the pressure, this may be written as an integral of a sum of terms, each of which is an n^{th} derivative of the product of a smooth function and the perturbation in sound speed multiplied by an integral of the squared eigenfunction. If the $(n-1)^{th}$ derivative of δc^2 is discontinuous, the n^{th} derivative in the integral

so obtained may be represented by a δ-function centred at the acoustic position of the discontinuity. If overshoot is present then $n=2$, while in its absence $n=3$. Hence the integral is replaced by the value of the integrand at this position, substituting the asymptotic expression for the eigenfunction, leading to an expression for the periodic component associated with δI (see Appendix A for the details of this derivation). The final result for the periodic signal in the frequency can be written as

$$\delta\omega_p \sim A(\omega,l)\cos\left[2\omega\int_{r_d}^{R}\left(1-\frac{S_l^2}{\omega^2}\right)^{1/2}\frac{\mathrm{d}r}{c}+2\phi\right]. \qquad (6)$$

(Note that we have dropped the subscript "0" in ω_0 since no confusion is likely to arise.) The amplitude $A(\omega,l)$ is in general a function of frequency, degree and of the local structure at the position r_d of the discontinuity. It follows from the analysis in Appendix A that, to leading order, A may be considered independent of l; if overshoot is present, A is approximately proportional to ω^{-1}, whereas $A\propto\omega^{-2}$ if the transition occurs for the Schwarzschild condition. The phase ϕ comes both from the effect of the upper turning point on the frequency of the modes and from the behaviour at the discontinuity; it is in general function of ω and l. In the case of overshoot, ϕ is smaller by $\pi/4$ than for no overshoot.

For future reference we define here the argument of the signal as

$$\Lambda(\omega,l)=2\omega\int_{r_d}^{R}\left(1-\frac{S_l^2}{\omega^2}\right)^{1/2}\frac{\mathrm{d}r}{c}+2\phi\,. \qquad (7)$$

To illustrate the physical reason for the presence of the oscillatory signal we now consider a simple problem of a potential well. The advantage of this example, with an analytical solution, is that the analogy with stellar oscillations can be easily established.

For $l=0$ the eigenfunctions of the modes of oscillation for the Sun satisfy asymptotically an equation of the type

$$\frac{\mathrm{d}^2Y}{\mathrm{d}\tau^2}+\left[\omega^2-V^2(\tau)\right]Y=0 \qquad (8)$$

(e.g. Vorontsov & Zharkov 1989), where $V(\tau)$ is an acoustic potential (independent of ω) and $Y(\tau)$ is the oscillation eigenfunction. Figure 1 shows the potential for two solar models: one without and the other with overshoot at the base of the convection zone as described in Sect. 5. This potential includes terms in the first and the second derivative of the sound speed. Hence any discontinuity in the first derivative of the sound speed gives rise to a δ-function in V, while a discontinuity in the second derivative of the sound speed causes a step function in V. Clearly, since V depends on the structure of the star, the exact solution of Eq. (8) can be obtained only numerically for a realistic model.

To simulate the effect on ω of a discontinuity we consider instead simpler problems by defining potentials for which we can determine an exact solution. The reference state is determined by a constant potential V_a (much smaller than ω) in the interval between 0 and τ_t, with eigenvalue ω_0. Next, we define

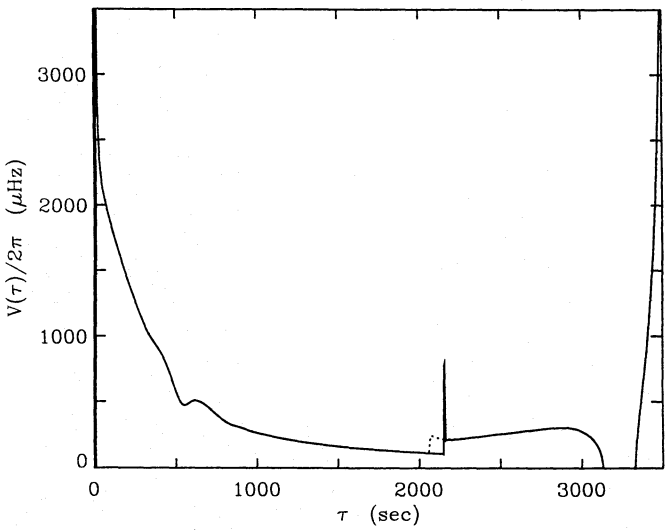

Fig. 1. Acoustic potential $V(\tau)$, τ being the acoustic depth, for two Models: a non-overshoot model (Y_1 - dotted line) and an overshoot model (Z_2 - continuous line). Both potentials are for $l=0$

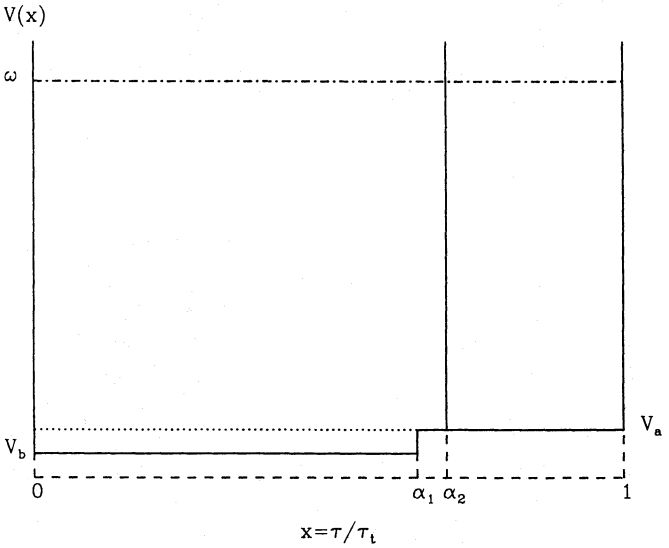

Fig. 2. Example of a potential which is constant everywhere in the interval $[0,\tau_t]$ and two types of perturbation: a step at $\alpha_1\tau_t$ and a δ function at $\alpha_2\tau_t$

two perturbations to this potential: one reducing its value to V_b between 0 and $\alpha_1\tau_t$; and the other adding a δ-function at $\alpha_2\tau_t$ $(0<\alpha_i<1)$ (see Fig. 2). These changes cause perturbations to ω_0 with periodic components given by

$$\delta\omega_{p1}\sim\frac{\delta V^2}{4\tau_t\omega_0^2}\sin\left[2\int_0^{\alpha_1\tau_t}(\omega_0^2-V_a^2)^{1/2}\mathrm{d}\tau\right] \qquad (9)$$

and

$$\delta\omega_{p2}\sim\frac{A_\delta}{2\tau_t\omega_0}\cos\left[2\int_0^{\alpha_2\tau_t}(\omega_0^2-V_a^2)^{1/2}\mathrm{d}\tau\right], \qquad (10)$$

respectively, where $\delta V^2 = V_a^2 - V_b^2$ is the step in the former potential and A_δ the amplitude associated with the δ-function in the latter. (See Appendix B for the details of the calculation.)

The nature of the signal in the frequencies for these simple cases is very similar to the result obtained for a star. Note the difference in the phase, and in the power of ω_0 in the amplitude, of the signal, depending on whether the potential has a step or a δ-function. If many mode frequencies are available, we can in principle distinguish between the two types of potential on the basis of the phase and the frequency dependence of the amplitude, and determine δV^2 and $\alpha_1 \tau_t$ in the first case, or A_δ and $\alpha_2 \tau_t$ in the second case, hence obtaining the nature, position and magnitude of the perturbations.

The method used to obtain expressions (9) – (10) can also be used for a star (e.g. Roxburgh & Vorontsov 1993; Basu et al. 1993). In this approach, suitable matching conditions on the eigenfunction are imposed at the base of the convective envelope.

3. Moderate-degree data and surface effects

Clearly, for low-degree data Eq. (7) gives that $\Lambda \sim 2\omega\tau_d + 2\phi$ to a first approximation. Hence we obtain a simple periodic signal with period equal to twice the acoustic depth $\tau_d = \tau(r_d)$ of the discontinuity, the acoustic depth at radius r being defined as

$$\tau(r) = \int_r^R \frac{\mathrm{d}r}{c} \,. \tag{11}$$

This kind of periodic signature was identified in the frequencies of a solar model by Gough (1990) using *second differences*, and was also investigated by Thompson (1988), Vorontsov (1988), and Gough & Sekii (1993). Such a periodic signal may in principle provide information for stars other than the Sun, where only low-degree modes are expected to be observed. It would indicate the presence of an abrupt transition in the star, and with sufficient observational precision the nature of the transition and its acoustic position may be constrained.

However, as discussed by Monteiro et al. (1993a,b), current low-degree solar data have a noise level higher than the amplitude expected for the solar signal given by Eq. (6), and hence cannot be used for our analysis. This indicates the necessity of including moderate-degree data, although evidently restricted to modes with their lower turning point below the base of the solar convective envelope; with existing observations, modes in the range $5 \leq l \leq 20$ are suitable. If such data are included, the analysis based on a simple periodic signal proves to be inadequate.

This is illustrated by Fig. 3a, which shows how the coherent behaviour of low-degree data is destroyed due to the effect of the l dependence. This has two possible sources. One arises because the amplitude $A(\omega, l)$ of the signal is a function of both degree and frequency. However, this effect is at most of order S_l^2/ω^2; hence, for modes with small S_l/ω it is negligible. In principle, the l-dependence could be taken into account by including in the expression for the amplitude a new parameter $\mathscr{P} = [c(r_d)/r_d]^2$,

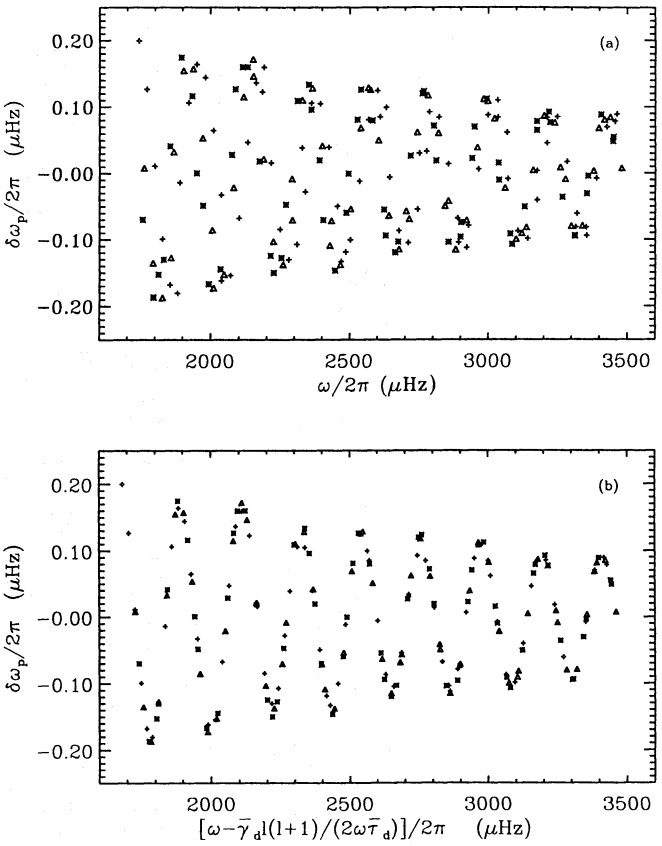

Fig. 3. a Signal versus frequency for Model Z_1 (cf. Table 1) and **b** the same signal but now plotted against $\omega - \bar{\gamma}_d L^2/2\omega\bar{\tau}_d$ to show the corrective effect of including $\bar{\gamma}_d$ (cf. Eq. (19)). The symbols are: ($\star$) l=5−10, ($\triangle$) l=11−15, and (+) l=16−20

in accordance with Eqs. (A29), (A6) in Appendix A for the dependence of $A(\omega, l)$ on l; this parameter should then be determined as part of the fit. However, because the effect of this term is very small for almost all the modes used in this analysis the fit does not improve substantially; consequently, we choose to neglect it, writing $A = A(\omega)$. Specifically, based on the behaviour expected in the case of no overshoot and overshoot, we express the amplitude as a sum of two terms, one proportional to ω^{-1} and one proportional to ω^{-2}:

$$A(\omega) = a_1 \left(\frac{\tilde{\omega}}{\omega}\right)^2 + a_2 \left(\frac{\tilde{\omega}}{\omega}\right) \,, \tag{12}$$

where a_1 and a_2 are constants and for convenience we have introduced $\tilde{\omega}/2\pi = 2500\,\mu$Hz.

The second contribution to the l-dependence is a phase shift; geometrically this arises because as l increases the ray paths through the convection zone depart more and more from the vertical, so that the path length from the surface to the discontinuity becomes longer. In order to use moderate-degree modes, without destroying the signal, we must account for this shift by including a first-order correction in Λ. Writing

$$\left(1 - \frac{S_l^2}{\omega^2}\right)^{1/2} \simeq 1 - \frac{S_l^2}{2\omega^2} - \frac{S_l^4}{8\omega^4} + \ldots \,, \tag{13}$$

it follows that to first approximation we have

$$\Lambda \simeq 2\omega \int_{r_d}^{R} \left(1 - \frac{S_l^2}{2\omega^2}\right) \frac{\mathrm{d}r}{c} + 2\phi \,. \tag{14}$$

Therefore,

$$\Lambda \simeq 2\omega\tau_d - \gamma_d \frac{L^2}{\omega} + 2\phi \,, \tag{15}$$

where

$$\gamma_d = \int_{r_d}^{R} \frac{c}{r^2} \mathrm{d}r \,. \tag{16}$$

Figure 3b shows the effect of introducing γ_d. Evidently this accounts for essentially the full l-dependence of the signal, which demonstrates that the phase shift is the dominant cause of the disorderly appearance of Fig. 3a. This may also be argued as follows. It is shown in Appendix A that the relative contribution to the amplitude from the degree is of order S_l^4/ω^4 if overshoot is present and $S_l^2/2\omega^2$ if it is not. Consider then the ratio of the latter to the change in $\delta\omega_p$ arising from the l-dependence of the phase (Eq. 14). This ratio may be shown to be approximately $(c/r)^2/(2\omega\gamma_d)\cot\Lambda \approx (1/20)(\tilde{\omega}/\omega)\cot\Lambda$. Except when ω is very small or $\cot\Lambda$ happens to be large, the ratio is small and so the change in phase dominates.

Additional difficulties arise from the contribution of the surface layers to the characteristics of the mode; here the simple asymptotic analysis breaks down, and in addition the uncertain effects of turbulent convection and energy transfer modify the properties of the oscillations. Consequently, as mentioned above, ϕ becomes a function of frequency and degree (Gough & Vorontsov 1993). Hence the determination of τ_d and γ_d will be affected. However, modes with degree $l \leq 20$ propagate almost vertically near the surface, so the l-dependence should be weak. Thus we write

$$\phi(\omega, l) = \phi_0 + a_\phi \omega + a_\gamma \frac{L^2}{2\omega} \,, \tag{17}$$

where ϕ_0, a_ϕ and a_γ are constants. Here the ω-dependence has been approximated as being linear, and we have retained only the l-dependent term that is functionally indistinguishable from the term in γ_d [as defined in Eq. (15)]. Substituting this into Eq. (15) it follows that

$$\Lambda \simeq 2\omega\overline{\tau}_d - \overline{\gamma}_d \frac{L^2}{\omega} + 2\phi_0 \,, \tag{18}$$

where we introduced

$$\overline{\tau}_d = \tau_d + a_\phi \quad \text{and} \quad \overline{\gamma}_d = \gamma_d + a_\gamma \,. \tag{19}$$

Finally, this gives the following expression for the signal:

$$\delta\omega_p \sim A(\omega) \cos\left(2\omega\overline{\tau}_d - \overline{\gamma}_d \frac{L^2}{\omega} + 2\phi_0\right) \,, \tag{20}$$

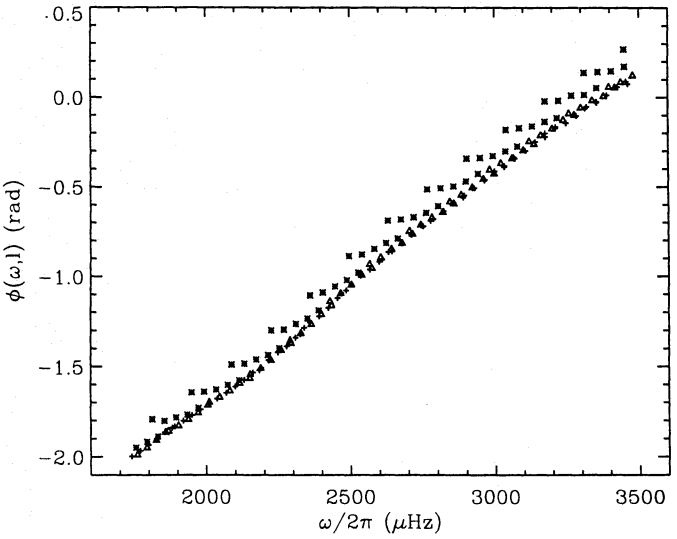

Fig. 4. Plot of the phase function $\phi(\omega, l)$ for Model Y_1 obtained from the acoustic phase α, determined by using the Duvall law (Christensen-Dalsgaard & Pérez Hernández 1992). Symbols as in Fig. 3

with $A(\omega)$ given by Eq. (12).

For a model of known structure, and assuming adiabatic oscillations, ϕ can be determined. The result is shown in Fig. 4, for one of the models discussed in Sect. 5. From these results we may estimate the value of a_ϕ to be of the order of 200 s (see Table 1). Evidently, any determination of $\overline{\tau}_d$ will only give τ_d if a_ϕ is known. However, asymptotically $\phi \sim \pi/4 - \pi\alpha(\omega, l)$, and hence

$$a_\phi \sim -\pi \frac{\mathrm{d}\alpha}{\mathrm{d}\omega} \,, \tag{21}$$

where $\alpha(\omega, l)$ is the phase function in the Duvall law (cf. Christensen-Dalsgaard & Pérez Hernández 1992). As is well known, $\mathrm{d}\alpha/\mathrm{d}\omega$ is undetermined observationally, and hence the period of the signal does not pin down the location of the discontinuity: unless model-dependent information is used, the determination of the location in acoustical depth is in error by an amount of order a_ϕ, i.e., about 200 s.

We also note here the difficulty of inferring radial distance from acoustic depth due to the uncertain treatment of the stellar surface layers. Because $|\mathrm{d}\tau/\mathrm{d}r| \equiv c^{-1}$ is relatively large there, any error in the physics of the last few per cent of the star is substantially amplified in the radius determined from the acoustic depth. However, if an accurate measurement of γ_d is achieved this difficulty may be partially overcome. The reason is that γ_d, given by Eq. (16), is relatively insensitive to the surface layers of the star. Near $r = R$, the sound speed is much smaller than in the interior, which together with the factor $1/r^2$ reduces the effect of the uncertain outermost parts of the star's structure on the value of γ_d. The effect of a_γ must also be taken into account; but we may clearly hope to be able to use this method to constrain further the value of r_d for the Sun from solar frequency data.

Table 1. Characteristics of the models. The letter Y corresponds to models without overshoot while Z is used for models with overshoot (see text). Column 2 gives the radial location of the base of the nearly adiabatically stratified region (including overshoot), and column 3 gives the radial location of the base of the convectively unstable envelope according to the Schwarzschild criterion. The acoustic depth corresponding to r_d is given by τ_d (see Eq. 11) while γ_d is determined as defined in Eq. (16). The quantities a_ϕ and a_γ (cf. Eq. 17), were calculated for each model by linear least-squares fitting of $\phi(\omega, l)$. **Notes: 1.** Model has reduced surface opacity, with $\delta \log \kappa = -0.3$ for $\log T \lesssim 4.2$. **2.** Model has a broad opacity increase, with $\delta \log \kappa = 0.093$ for $5 \lesssim \log T \lesssim 6.8$, in order to increase the depth of the convection zone. **3.** Model has higher opacity immediately beneath the convection zone, with $\delta \log \kappa = 0.093$ for $5 \lesssim \log T \lesssim 6.4$

Model	r_d/R	r_c/R	τ_d (s)	a_ϕ (s)	$\gamma_d/2\pi$ (μHz)	$a_\gamma/2\pi$ (μHz)	Notes
Y_1	.7287	.7287	2068	201	12.10	-1.43	-
Y_{1a}	.7289	.7289	2059	196	12.20	-1.45	1
Y_2	.7132	.7132	2121	199	13.59	-1.43	2
Y_3	.7149	.7149	2116	201	13.54	-1.40	3
Z_1	.7132	.7283	2117	201	13.58	-1.43	-
Z_2	.6994	.7273	2160	201	15.01	-1.44	-
Z_{2a}	.6999	.7275	2147	197	14.99	-1.45	1

4. Method to isolate the signal

In this section we outline the method developed to isolate the signal given by Eq. (20) and hence determine the parameters $\overline{\tau}_d$, $\overline{\gamma}_d$, ϕ_0 and the function $A(\omega)$. Full details of our numerical procedure are given in Appendix C.

The basic idea is to fit all points ω_{nl}, for a given l, by a smooth function such as to leave in the residuals only the signal we are studying. The best values of the parameters for the signal are then obtained through a simultaneous least-squares fit to the residuals for different l.

The smooth function must eliminate all variations of ω_{nl} on scales substantially longer than the contribution from the base of the convection zone which we wish to isolate, without affecting the characteristics of the latter. Oscillatory components in the frequencies arise from any region where the solar structure undergoes rapid variations. Particularly significant is the region of second helium ionization near the surface, where the adiabatic exponent $\Gamma_1 = (\partial \ln p/\partial \ln \rho)_s$ (the derivative being at constant specific entropy s) changes rapidly on a short scale. This produces a corresponding signature in the sound speed, and hence induces an oscillatory signal in the frequencies, which is conceptually similar to the one we are considering although differing in the period and amplitude behaviour. Such contributions are responsible for the difficulties surrounding the isolation of the signal from the base of the convection zone; care is required to avoid that they contaminate the inferred values of the parameters. As described in Appendix C, this is achieved in our method through a gradual relaxation of the condition of smoothness in the fit; as a result, we are able to make a reliable determination of the parameters associated with the base of the convection zone. [We note that the oscillatory signal coming from the second helium ionization zone has proven to be a powerful measure of the helium abundance and a diagnostic of the equation of state; e.g. Christensen-Dalsgaard & Pérez Hernández (1991); Vorontsov et al. (1991, 1992).]

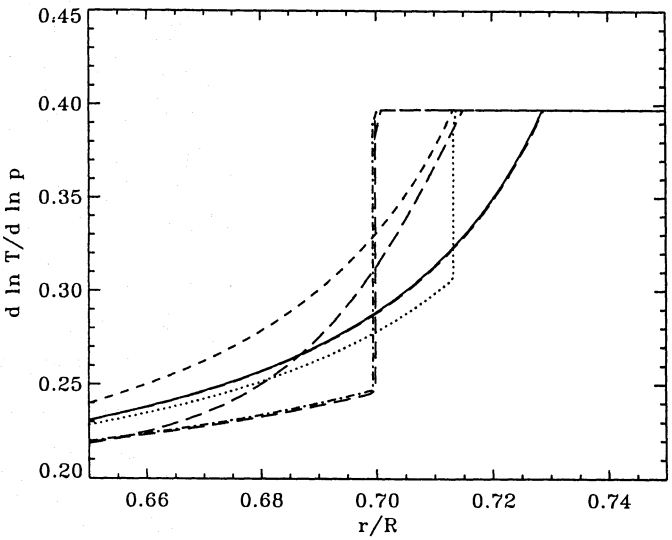

Fig. 5. Temperature gradient ∇ at the base of the convective envelope for models: Y_{1a} (continuous line), Y_2 (dashed line), Y_3 (long-dashed line), Z_1 (dotted line), Z_2 (dot-dashed line). Temperature gradients for models Y_1 and Z_{2a} are also depicted, but these are virtually indistinguishable in the figure from those of models Y_{1a} and Z_2 respectively

5. Models

To test the method we use a number of theoretical models (see Table 1). Apart from the inclusion of overshoot, the models were calculated essentially as described by Christensen-Dalsgaard (1982), although with substantially higher numerical precisions and using opacities based on the Los Alamos Opacity Library. For simplicity, full evolution sequences were not computed; instead the hydrogen abundance was obtained by scaling from a suitable model of the present Sun, the scaling factor being determined, together with the mixing-length parameter, to obtain the correct solar luminosity and radius (cf. Christensen-Dalsgaard & Thompson 1991).

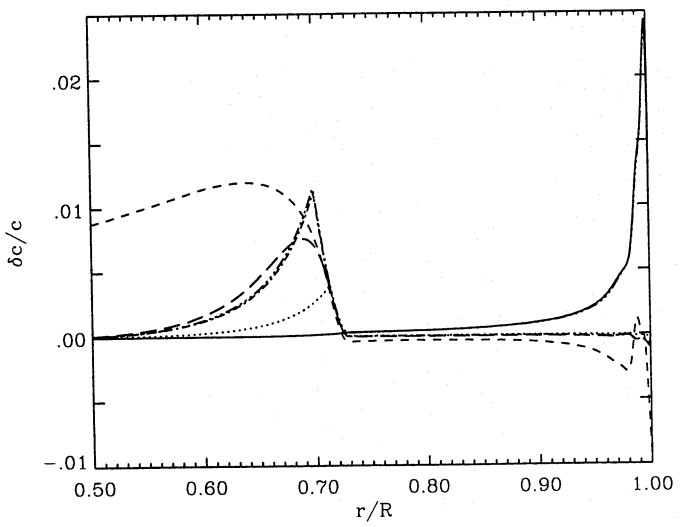

Fig. 6. Relative sound-speed differences $(c_i - c_1)/c_1$, at fixed r; here c_1 refers to Model Y_1, and c_i to the following Models: Y_{1a} (continuous line), Y_2 (dashed line), Y_3 (long-dashed line), Z_1 (dotted line), Z_2 (dot-dashed line), Z_{2a} (triple dot-dashed line)

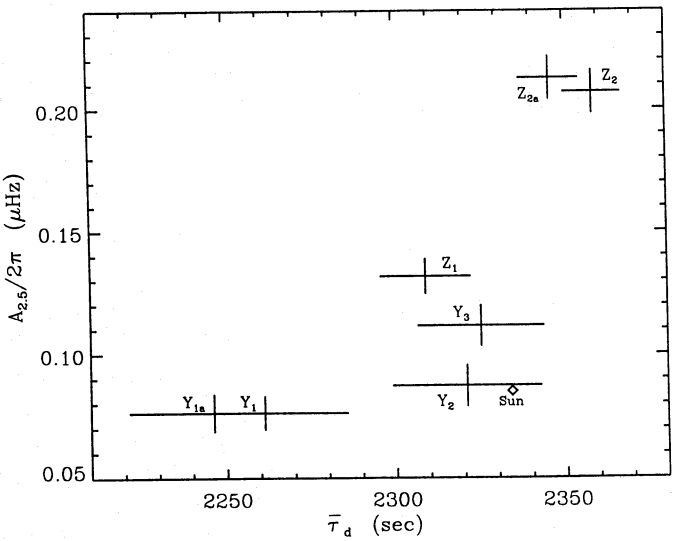

Fig. 7. Amplitude $A_{2.5}$ of the signal, in terms of cyclic frequency, at $\omega/2\pi = 2500\,\mu$Hz, versus $\bar{\tau}_d$ for all models. The error bars are the standard deviation obtained for 100 realizations of randomly generated errors for each model. (◇) corresponds to the values found for the solar data of Libbrecht et al. (1990)

Models Z_1 Z_2 and Z_{2a} have overshoot, Z_1 being the least extreme. In order to study the applicability of the method proposed we have implemented overshoot in the simplest possible way, through a model which simulates the results of more detailed calculations, with a few adjustable parameters which may be used to specify the extent of overshoot and the thickness of the transition zone. Specifically, the actual temperature gradient $\nabla = \mathrm{d}\ln T/\mathrm{d}\ln p$ is related to the adiabatic gradient ∇_{ad} and the radiative gradient ∇_{rad}, through

$$\nabla_{\mathrm{ad}} - \nabla = \frac{\nabla_{\mathrm{ad}} - \nabla_{\mathrm{rad}}}{1 + \mathscr{C}\,[\mathscr{D} - (\nabla_{\mathrm{ad}} - \nabla_{\mathrm{rad}})]} \qquad (22)$$

when $0 < \nabla_{\mathrm{ad}} - \nabla_{\mathrm{rad}} < \mathscr{D}$; in the convection zone ∇ is computed from the usual mixing-length expression. Here $\mathscr{D}$ and $\mathscr{C}$ are adjustable parameters, determining the extent of overshoot and the thickness of the transition region to radiative stratification, respectively. This expression clearly has the desired form; also it might be noted that the expression is purely local, and hence easily implemented. We have used $\mathscr{C} = 10^5$ (giving a very abrupt transition), and values of $\mathscr{D}$ chosen to obtain the desired depths of the overshoot region.

The other models do not have overshoot. Model Y_1 is a "standard" solar model. The remaining models incorporate localized changes in the opacity, defined as in Eqs (3) and (4) of Christensen-Dalsgaard & Thompson (1991). Model Y_3 is distinguished by having a localized opacity increase, relative to the other models, near the base of the convection zone, to see whether this can distinguished from overshoot. Model Y_2 has a broader opacity change in order to increase the depth of the convective envelope relative to Y_1 such that its base is at the location of the base of the overshoot region in Model Z_1.

Figure 5 shows ∇ for some of the models considered, both without and with overshoot.

To test the effect of near-surface uncertainties, Models Y_{1a} and Z_{2a} differ from Y_1 and Z_2 in having different atmospheric opacities and hence different frequencies and phases ϕ. This causes the acoustic depth of the base of their adiabatic region to be slightly different from that in the corresponding model without opacity modification, though the atmospheric change hardly affects the depth in terms of radius.

The difference in adiabatic sound speed is important for understanding the differences in the model frequencies. Figure 6 therefore shows relative sound-speed differences, at fixed radius, between several models and Model Y_1.

6. Results for artificial data

In testing the method we used a set of 197 frequencies of modes with degrees in the range $5 \leq l \leq 20$, the same set as was used in the analysis of the solar data (see Sect. 7 below). For each model the frequencies of oscillation were calculated. We first applied our procedure to these "data" to test it in the absence of errors. Then, to determine the effect of observational errors on our inferences we constructed 100 realizations of randomly generated errors and added these to the numerical frequencies of each model. The errors were independent and normally distributed with zero mean and standard deviations (which differed from one mode to another) given by the estimated uncertainties for the observational data (see below). Table 2 lists the inferred values in the error-free case of the parameters of the fit and also the mean values and standard deviations for the realizations with errors. Figure 7 is a plot of a representative value of the amplitude against $\bar{\tau}_d$.

As expected, the inferred amplitudes of the signal are largest for the models with overshoot, particularly for Models Z_2 and

Table 2. List of the inferred values of $A_{2.5}/2\pi$ (μHz) ($A_{2.5}$ being the amplitude A evaluated at $\omega/2\pi$ =2500 μHz), $\bar{\tau}_d$ (s), $\bar{\gamma}_d/2\pi$ (μHz) and ϕ_0 (rad), from error-free frequencies and for 100 realizations of randomly generated errors, with the corresponding solar σ value added to the frequencies of the models. The values for the error-free case are shown as well as the standard deviation and mean values for the error realizations. The solar values inferred from the Libbrecht et al. (1990) data are also shown in the last row

Model	error free case				mean value				standard deviation			
	$A_{2.5}/2\pi$	$\bar{\tau}_d$	$\bar{\gamma}_d/2\pi$	ϕ_0	$A_{2.5}/2\pi$	$\bar{\tau}_d$	$\bar{\gamma}_d/2\pi$	ϕ_0	$\Delta A_{2.5}/2\pi$	$\Delta\bar{\tau}_d$	$\Delta\bar{\gamma}_d/2\pi$	$\Delta\phi_0$
Y_1	.075	2264	10.3	1.21	.076	2261	10.0	1.24	.007	25	2.3	.39
Y_{1a}	.075	2249	10.6	1.42	.076	2246	10.7	1.45	.008	25	2.4	.39
Y_2	.087	2322	12.6	1.06	.087	2321	12.6	1.10	.009	22	2.3	.45
Y_3	.111	2325	12.7	1.01	.112	2325	12.8	1.01	.009	19	1.8	.28
Z_1	.132	2307	12.0	0.84	.132	2309	11.8	0.81	.008	14	1.5	.22
Z_2	.207	2360	13.9	0.59	.207	2359	13.8	0.61	.009	9	1.1	.14
Z_{2a}	.212	2346	13.9	0.80	.213	2346	13.7	0.81	.009	9	1.0	.14
Sun					.085	2334	12.2	0.67				

Z_{2a} in which the extent of overshooting is greatest. The model with a localized increase in opacity (Y_3) also has a fairly large amplitude which, though smaller than that of any of the overshoot models, comes close to the amplitude for Model Z_1. Models with neither overshoot nor a very localized opacity increase have substantially smaller amplitudes.

Comparison of Tables 1 and 2 shows that, as explained in Sect. 3, the inferred "depth" $\bar{\tau}_d$ is a poor estimate of the actual acoustic depth τ_d of the base of the adiabatic layer but is rather an estimate of $\tau_d + a_\phi$ [cf. Eqs (17) and (19)]. For the models considered the values of a_ϕ are very similar, all being of the order of 200 s. Therefore the inferred value of $\bar{\tau}_d$ can adequately be corrected, within the accuracy of approximating ϕ by expression (17), to give an estimate of the actual acoustic depth.

The mean results from 100 realizations of data with random errors (Table 2) are in good agreement with the results from error-free data, indicating that random data errors do not introduce any significant systematic error into our procedure. Of course, the uncertainty in a single realization is very relevant to the interpretation of the results from observational data The standard deviations are reasonably modest. In particular, the uncertainty in the amplitude (less than 0.009) is small compared with the difference between "standard" models Y_1, Y_{1a}, Y_2 and the overshoot models. The uncertainty in the inferred $\bar{\tau}_d$ is of order 25 s for models without overshoot and less than 14 s for models with overshoot. (The systematic difference between the two groups is as one would expect, given that the signal amplitude for the overshoot models is greater, so that the signal's characteristics should be easier to determine.)

Figure 8 illustrates $(\omega/\tilde{\omega})^2 A(\omega)$ for some of the models. As predicted by Eq. (A29) the frequency dependence of the amplitude differs by a factor of ω between models with and without overshoot. This is particularly evident from a comparison of Models Z_1 and Y_3 where the overall level of the amplitude is similar; these results suggest that the frequency dependence of the amplitudes might be used to distinguish between overshoot and a localized change in the opacity. However, we caution that

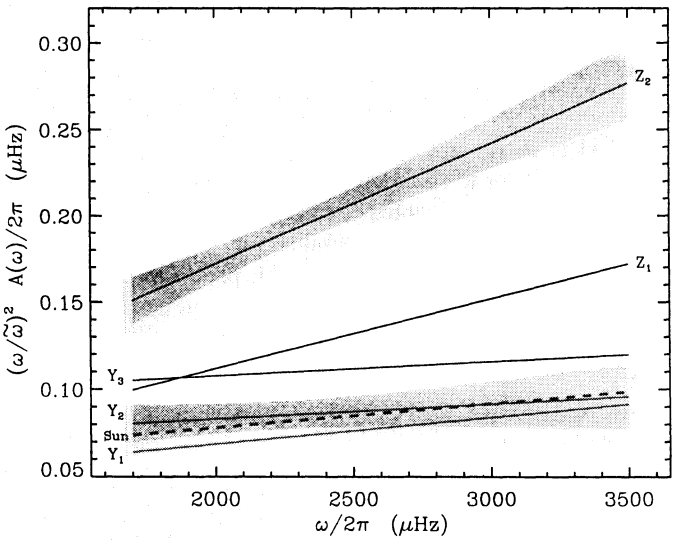

Fig. 8. Inferred amplitudes multiplied $(\omega/\tilde{\omega})^2$ (see Eq. 12) for all models; the shadowy areas show 1σ deviations obtained from 100 error realizations for Models Y_2 and Z_2 (all other models have a similar behaviour). The behaviour obtained for solar data is shown as a thick dashed line

the clear distinction in $A(\omega)$ for error-free data between overshoot and non-overshoot models can be blurred by the presence of data errors. The values of ϕ_0 (see Table 2) also show a systematic difference between models with and without overshoot, in accordance with expectations. However, it is clear from the results for Y_1 and Y_{1a} or Z_2 and Z_{2a} that its actual value is sensitive to the surface layers; this, together with the high uncertainties from observational errors, makes ϕ_0 of little use for analyzing the solar data.

7. Results for observational data

The solar data of Libbrecht et al. (1990) were used in this study. The modes were selected according to the criteria that they

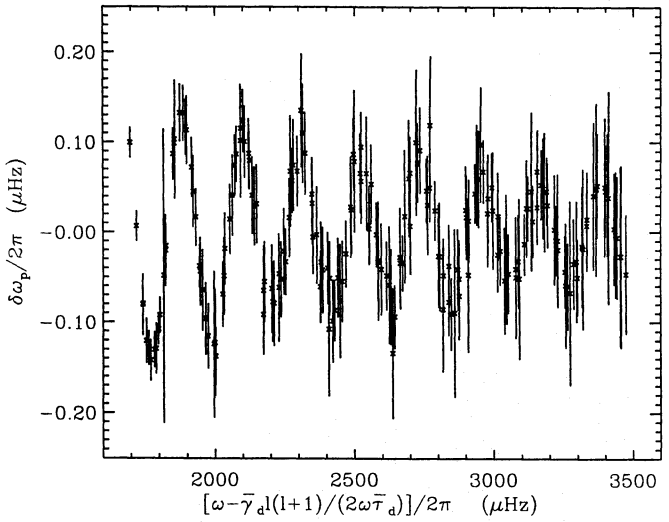

Fig. 9. Solar signal versus reduced frequency. The error bars correspond to the observational errors for the solar data

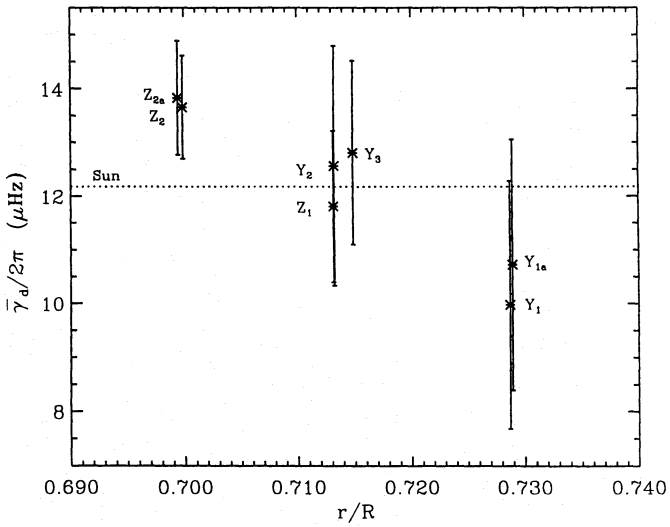

Fig. 10. Plot of $\bar{\gamma}_d$ versus the radial position of the base of the convective envelope in the models. The error bars correspond to the standard deviation for 100 error realizations while the dotted line is the value inferred for the solar data

should contain the base of the convective envelope well within their acoustic cavity, and that their observed frequencies should have relatively small errors. Thus we used modes with $5 \leq l \leq 20$ and $1700\,\mu\text{Hz} \leq \omega/2\pi \leq 3500\,\mu\text{Hz}$, which left a total of 197 modes, with a mean of the quoted errors of $0.05\,\mu$Hz. This set of modes was used also for the tests on models, described above, and the same procedures were used on both observational and artificial data.

The solar signal has been plotted in Fig. 9 against corrected frequency. Results of the fit are given at the bottom of Table 2 and are also shown in Fig. 7. The solar data have a lower amplitude than any of the overshoot models. Its amplitude is 12 standard deviations below the values for Z_2 and Z_{2a} (which have overshoot regions $0.03R$ in extent), and about 5 s.d. below Model Z_1, which has a $0.015R$ overshoot distance. On the other hand, the solar amplitude is over 1 s.d. greater than those of Models Y_1 and Y_{1a}, and is closest to the non-overshoot Model Y_2, both in terms of amplitude and $\bar{\tau}_d$. Although the statistical analysis is somewhat uncertain, we estimate from these results that overshoot of the nature considered here does not exceed $0.005R$ in the Sun, at a 95 per cent confidence level. From Fig. 8 it also appears that the solar data favours the frequency dependence of the amplitude shown by models without overshoot (i.e., $A(\omega) \propto 1/\omega^2$) instead of overshoot models (with $A(\omega) \propto 1/\omega$). Indeed, for the entire frequency interval considered the solar amplitude is within 1σ of the amplitude found for model Y_2.

As mentioned in Sect. 3, $\bar{\gamma}_d$ should in principle be less sensitive to the surface layers of the Sun, and therefore give a better estimate of the position of the base of the adiabatically stratified region, than $\bar{\tau}_d$. Figure 10 shows $\bar{\gamma}_d$ versus r_d for all models, with error bars given by the 1σ deviations found from the 100 error realizations. The value obtained for the solar data is shown as a dotted line. The observational errors clearly limit the accuracy with which we may currently determine the value of $\bar{\gamma}_d$; however, it seems to confirm that r_d is between $0.71R$ and $0.72R$, in accordance with the value found by Christensen-Dalsgaard et al. (1991). Obviously, this statement assumes that the contribution from a_γ can be considered as a shift in Fig. 10, not strongly affecting the relative positions on the plot. From Table 1, we see that $a_\gamma/2\pi$ varies from model to model by at most 0.05μHz. Provided the differences in the surfaces layers of the models reflect the possible differences between models and the Sun, we conclude that this corresponds to an uncertainty in r_d from $\bar{\gamma}_d/2\pi$ of about $5 \times 10^{-4}R$. This is much smaller than the uncertainty introduced in the determination of r_d from τ_d due to the uncertainties in the sound speed behaviour near the surface as determined from helioseismic inversions. We cannot exclude, however, that neglected effects in the near-surface layers of the Sun might make additional significant contributions to $\bar{\gamma}_d$, beyond those that have been considered here. Nonetheless, $\bar{\gamma}_d$, may well prove very useful as an extra position indicator, especially if more accurate data become available for the determination of $\bar{\gamma}_d$.

8. Differential method

An alternative approach to detecting the signature of convective overshoot in solar frequencies is to analyze the *differences* between the observed frequencies and those of a solar model (Berthomieu et al.1993; Monteiro et al.1993b). From simple asymptotics, which assume that the internal structure of the Sun and model vary only on scales large compared with the wavelength of the modes, one finds that the relative frequency differences (scaled by S, which describes the degree dependence of the mode inertia) are approximately the sum of a function of ω/L (where in this section we use the definition $L=l+1/2$) and a function of frequency:

$$S\,\frac{\delta\omega}{\omega} \simeq H_1(\omega/L) + H_2(\omega) \tag{23}$$

(Christensen-Dalsgaard et al. 1989). In particular, H_1 depends on the relative sound-speed difference between Sun and model (or between pairs of models):

$$H_1(w) \simeq \int_{r_t}^{R} \left(1 - \frac{c^2}{w^2 r^2}\right)^{-1/2} \frac{\delta c}{c}\,\frac{\mathrm{d}r}{c} \tag{24}$$

(with the integration from the point where the square root vanishes up to the surface). Differences in near-surface structure and mode dynamics contribute a fairly slowly-varying component to $H_2(\omega)$. If, however, there is a localized difference in sound speed then this will contribute an additional, more rapidly varying signal. As for the analysis in Sects. 2 and 3 above, this has the form of an oscillatory function of frequency if the perturbation is located near the base of the convection zone and only low degree modes are considered, while the inclusion of higher-degree modes will introduce a phase shift into the signal.

To illustrate how overshoot might be detected in frequency differences we consider pairs of theoretical models from amongst the models introduced in Sect. 5. As a proxy for the Sun we take the overshoot model Z_{2a}, and we consider the difference between its frequencies and those of three other models, namely Y_1, Y_3, and Z_2. Sound-speed differences for the various models were presented in Fig. 6. Frequency differences, scaled by S, for the three model pairs are shown in Fig. 11. The only structural differences between Z_{2a} and Z_2 are in the near-surface layers, so the scaled frequency differences are just given by the H_2 term in Eq. (23). This term also dominates the frequency differences for the other pairs, though the sound-speed difference between Z_{2a} and Y_1 is large enough for the contribution from H_1 to be quite visible in the figure as a spread in the frequency differences. On the other hand, although the difference between the sound speeds of Z_{2a} and Y_3 is evident in Fig. 6, its integrated effect on the frequency differences is rather small. Consequently a simple comparison of frequency differences (Fig. 11) cannot readily distinguish whether Z_{2a} more nearly resembles model Z_2 (with overshoot) or model Y_3, which has no overshoot but a localized opacity enhancement. This would be particularly the case if the data had errors.

The reason for the difficulty is that the differences in the surface regions give a substantial H_2, which masks more subtle variations coming from the base of the convection zone. This can be overcome by removing the surface contribution, using a two-spline fit (Christensen-Dalsgaard et al.1989). To illustrate how this works we consider further the scaled frequency differences between Models Z_{2a} and Y_1. The scaled differences less the fitted smooth H_2 are presented in Fig. 12a. The big jump around $\omega/2\pi L = 100\,\mu$Hz reflects the substantial difference in sound speed near the base of the convection zone, indicating that the models do not have adiabatically stratified regions of the same depth. The scatter for larger values of $\omega/2\pi L$ (i.e., for modes that penetrate beneath the convection zone) shows that the models have a sharp difference in sound speed at some radius. The extent of this scatter is clearer in Fig. 12b, which shows the scaled differences less the sum of H_1 and H_2. The periodic nature of these residues is manifest there if only degrees l=0–5 are taken (dashed line).

The periodicity of the residuals to the asymptotic fit is analogous to the periodic signal sought in the absolute method. The drawback to this differential approach is that even if it is not sharp a localized sound-speed difference due to a mismatch in convection-zone depths tends to contribute to the apparent signal. A strategy therefore might be to reduce the substantial step in H_1 at $\omega/2\pi L \simeq 100\,\mu$Hz by finding a model that has an adiabatic region of the correct depth, and then to use the scatter for more deeply penetrating modes to distinguish whether the remaining difference is sharp or fuzzy. We have not yet pursued this further, however.

9. Conclusion

In this work we propose two methods for studying overshoot at the base of the solar convection zone, using seismic data. The first, an absolute method, consists in using directly the signature of this region on the frequencies of oscillation. From the variational principle for linear, adiabatic nonradial oscillations an expression for this signal was determined, valid also for moderate-degree data. The expected amplitude of the signal was calibrated as a function of the abruptness of the transition by using solar models with different characteristics at the base of their convective envelopes. In this way we may put an upper limit to the depth of convective overshoot at the base of the solar convective envelope of $0.005R$ (corresponding to $0.07H_p$, where H_p is the local pressure scale height) with a 95 per cent confidence level.

As theoretically expected, there is also a different frequency dependence of the amplitude between models with and without overshoot. Here again, the solar data favour the behaviour found for models without overshoot.

Our results are consistent with the findings of Basu et al. (1993) who extended the idea of using second differences of frequencies to higher-order differences. Provided this is not taken too far, it enhances the signal from the base of the convection zone without the effect of data errors becoming dominant. Basu et al. conclude that a two-sigma upper limit of $0.1H_p$ can be placed on the extent of overshoot, in close agreement with our result.

It must be noted, however, that our analysis assumed a spherically symmetric solar model. In reality, the overshoot probably has the form of plumes with a distribution of penetration depths in space and time; hence, although each plume quite likely exhibits the structure obtained in simple models, with a nearly adiabatic region followed by an abrupt transition to radiative transport, the average structure felt by the modes of oscillation is likely to be more fuzzy. Additional apparent fuzziness might result from a possible oblateness of the base of the convection zone. Therefore, if on physical grounds we prefer to assume that overshoot must be present, the results obtained here should be interpreted as constraining the simplest possible model, with

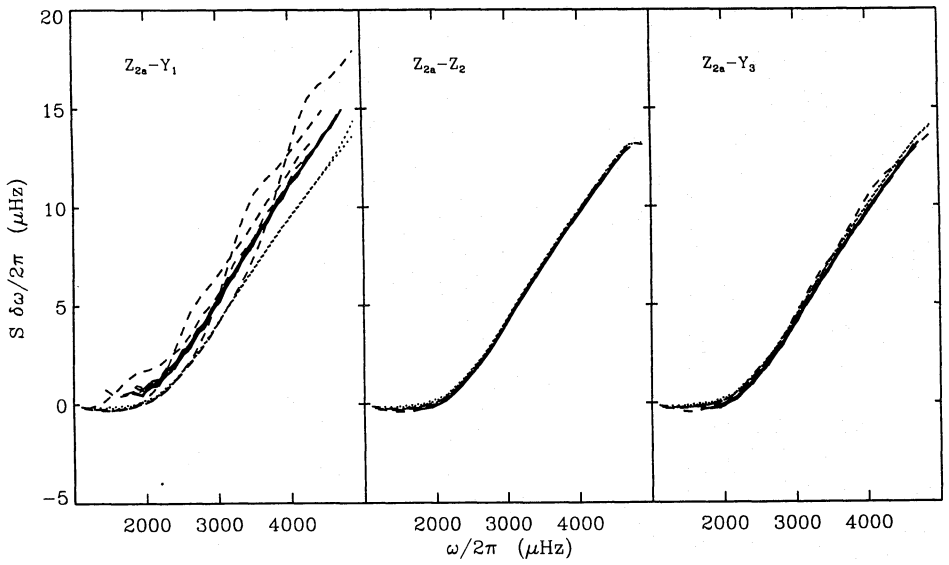

Fig. 11. Frequency differences between Models Z_{2a} and Z_1 versus $\omega/2\pi$. The differences have been scaled by the mode inertia S, normalized at each frequency such as to be unity for radial modes. Lines connect points with the same value of l, with the style: (solid) $l = 0, 1, 2, 3, 4, 5$; (dashed) $l = 10, 20, 30, 40, 50$ and (dotted) $l = 70, 100$

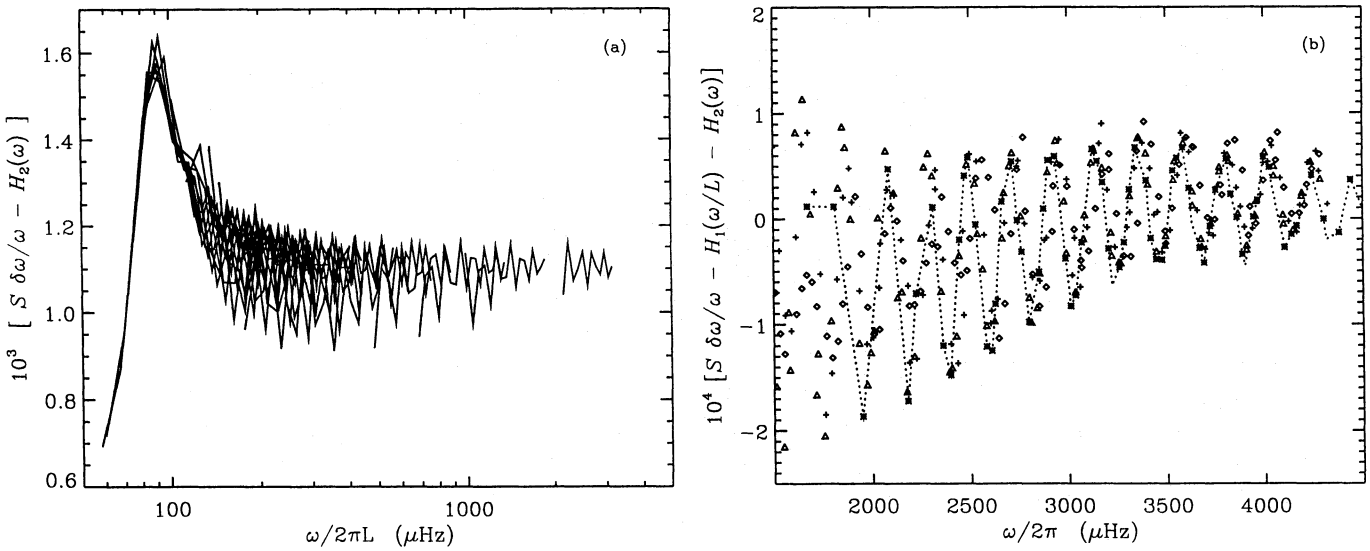

Fig. 12. a Scaled frequency differences between Models Z_{2a} and y_1, less $H_1(\omega)$ (defined in Eq. 24). Solid lines connect points with same l value. **b** Same differences, less both the components $H_1(\omega)$ and $H_2(L/\omega)$ (Eq. 23). The dotted line connects points with $l = 0-5$ which are represented by ($\star$), while the other symbols are ($\triangle$) $l = 6-10$, (+) $l = 11-15$ and ($\diamond$) $l = 16-20$

overshoot extending the adiabatically stratified region below the Schwarzschild boundary, with a sharp spherically symmetric transition to the stratification corresponding to radiative energy transport. With improved data, we may hope to place tighter constraints on the transition from adiabatic to radiative stratification, and in this way test average properties of more realistic hydrodynamical models for convective overshoot.

The other important information potentially provided by the analysis of the solar data is the radial position r_d of the transition. But, as shown, in the oscillatory signal the acoustic position occurs in combination with a term resulting from the effect of the surface layers; here the turning point depends on the frequency of the mode, causing a phase shift that is frequency dependent and observationally undetermined. Furthermore, to determine radial position from acoustic depth, accurate knowledge of the sound speed near the surface is required. We point out that a different parameter of the fitting carries information about the location of the transition, while being less sensitive to uncertainties near the surface. However, since it is of higher order than τ_d in the expansion of the signal, it is more strongly affected by current observational errors, limiting the precision of the r_d determination to worse than $0.005R$. To this accuracy, the results confirm the value determined by Christensen-Dalsgaard et al. (1991). We also note that the absolute value of γ_d is affected by the l-dependence of the surface phase; however, our model calculations indicate that this is unlikely to produce a significant relative difference between the models and the Sun when going from γ_d to $\overline{\gamma}_d$. Therefore, in determining r_d from relative values of $\overline{\gamma}_d$ the expected error from this source is less than $5 \times 10^{-4}R$. In addition, the neglect of the dependence of

the signal amplitude on degree will mainly affect $\overline{\gamma}_d$ amongst the parameters considered in the fit; however, as discussed in Appendix A this effect is also very small. Therefore, the determination of r_d discussed above is not changed significantly by these uncertainties, in comparison with present observational errors.

The second method is a differential technique, based on analyzing frequency differences between two models, or between a reference model and the Sun. Using such a technique, Berthomieu et al. (1993) inferred the presence of overshoot in the Sun. However, Monteiro et al. (1993b) pointed out that simple inspection of the frequency differences cannot distinguish between effects of overshoot and, e.g., localized errors in the opacity. Here we find, using an asymptotic decomposition of suitably scaled differences, that it is possible with proper choice of reference model to isolate an oscillatory signal which reflects the presence of overshoot. On the other hand, given the potential sensitivity of the result on the properties of the reference, we feel that the absolute method of analysis, properly calibrated against results obtained from the frequencies of theoretical models, is preferable for this problem.

Acknowledgements. MJPFGM is co-supported by grant *BD–1274/91–RM* from *Junta Nacional de Investigação Científica e Tecnológica* – Portugal. The computations reported here were supported by the Danish Natural Science Research Council. JC-D and MJT are grateful to the High Altitude Observatory for hospitality during part of this project.

Appendix A: variational analysis

We start from Eq. (5) for δI in terms of the perturbations $\delta\rho$ and $\delta(\rho c^2)$ and the equilibrium structure of the smooth star. The horizontal component of the displacement vector is eliminated by substituting

$$\xi_h = \frac{1}{\omega^2 - S_l^2}\left[\frac{g}{r}\xi_r - \frac{c^2}{r^3}\frac{\mathrm{d}(r^2\xi_r)}{\mathrm{d}r}\right] . \qquad (A1)$$

Furthermore, we replace integration over r by integration over acoustic depth τ defined by $\mathrm{d}\tau = -\mathrm{d}r/c$ and $\tau = 0$ at $r = R$; we also truncate the integration at the lower turning point r_t of the mode (corresponding to $\tau = \tau_t$), since the eigenfunction is very small below this point. The result is an expression of the form

$$\delta I = \int_0^{\tau_t}\left[f_1(r)E_r^2 + f_2(r)\frac{dE_r^2}{\mathrm{d}\tau} + f_3(r)\left(\frac{dE_r}{\mathrm{d}\tau}\right)^2\right]\mathrm{d}\tau\ ; \qquad (A2)$$

here the f_i's are functions of the background state and the perturbations $\delta\rho$ and $\delta(\rho c^2)$. Also, E_r is a scaled eigenfunction given by

$$E_r = r\sqrt{\rho c}\ \xi_r . \qquad (A3)$$

The scaling factor is introduced in order to remove from ξ_r the radial dependence of the amplitude within the propagating region. We now use

$$\left(\frac{dE_r}{\mathrm{d}\tau}\right)^2 = \frac{1}{2}\frac{\mathrm{d}^2E_r^2}{\mathrm{d}\tau^2} - E_r\frac{\mathrm{d}^2E_r}{\mathrm{d}\tau^2} , \qquad (A4)$$

and substitute the asymptotic result

$$\frac{\mathrm{d}^2E_r}{\mathrm{d}\tau^2} \simeq -\omega^2(1-\Delta)\,E_r , \qquad (A5)$$

with

$$\Delta \equiv \frac{S_l^2}{\omega^2} = \frac{l(l+1)c^2}{\omega^2 r^2} , \qquad (A6)$$

to obtain

$$\delta I = \int_0^{\tau_t}\left(\delta B_1\,E_r^2 + \delta B_2\frac{\mathrm{d}E_r^2}{\mathrm{d}\tau} + \delta B_3\frac{\mathrm{d}^2E_r^2}{\mathrm{d}\tau^2}\right)\mathrm{d}\tau + \int_0^{\tau_t}\frac{\mathrm{d}\delta B_0}{\mathrm{d}\tau}E_r^2\mathrm{d}\tau . \qquad (A7)$$

Here

$$\delta B_0 = \frac{g}{c}\frac{\delta c^2}{c^2} - \frac{g}{c}\frac{\delta(\Gamma_1 p)}{\Gamma_1 p} , \qquad (A8)$$

$$\delta B_1 = \left\{-\frac{\omega^2}{1-\Delta} + \frac{g}{c}\frac{\mathrm{d}}{\mathrm{d}\tau}\log\left(\frac{g}{\rho c}\right) - \frac{1-2\Delta}{(1-\Delta)^2}\frac{g}{c}\frac{\mathrm{d}}{\mathrm{d}\tau}\log\left(\frac{r^2}{\rho c}\right) - \frac{1}{4}\frac{\Delta}{(1-\Delta)^2}\left[\frac{\mathrm{d}}{\mathrm{d}\tau}\log\left(\frac{r^2}{\rho c}\right)\right]^2 + \frac{\Delta(1-2\Delta)}{(1-\Delta)^2}\frac{g^2}{c^2}\right\}\frac{\delta c^2}{c^2} + \left\{\frac{g}{c}\frac{\mathrm{d}}{\mathrm{d}\tau}\log\left(\frac{g}{\rho c}\right) - \frac{1}{1-\Delta}\frac{g}{c}\frac{\mathrm{d}}{\mathrm{d}\tau}\log\left(\frac{r^2}{\rho c}\right) - \frac{1}{4}\frac{1}{1-\Delta}\left[\frac{\mathrm{d}}{\mathrm{d}\tau}\log\left(\frac{r^2}{\rho c}\right)\right]^2 + \frac{\Delta}{1-\Delta}\frac{g^2}{c^2}\right\}\frac{\delta(\Gamma_1 p)}{\Gamma_1 p} , \qquad (A9)$$

$$\delta B_2 = -\left\{\frac{1-2\Delta}{(1-\Delta)^2}\frac{g}{c} + \frac{1}{2}\frac{\Delta}{(1-\Delta)^2}\frac{\mathrm{d}}{\mathrm{d}\tau}\log\left(\frac{r^2}{\rho c}\right)\right\}\frac{\delta c^2}{c^2} - \left\{\frac{1}{1-\Delta}\frac{g}{c} - \frac{1}{2}\frac{1}{1-\Delta}\frac{\mathrm{d}}{\mathrm{d}\tau}\log\left(\frac{r^2}{\rho c}\right)\right\}\frac{\delta(\Gamma_1 p)}{\Gamma_1 p} , \qquad (A10)$$

$$\delta B_3 = -\frac{1}{2}\frac{\Delta}{(1-\Delta)^2}\frac{\delta c^2}{c^2} + \frac{1}{2}\frac{1}{(1-\Delta)^2}\frac{\delta(\Gamma_1 p)}{\Gamma_1 p} . \qquad (A11)$$

We have used

$$\frac{\delta(\Gamma_1 p)}{\Gamma_1 p} = \frac{\delta(\rho c^2)}{\rho c^2} \qquad (A12)$$

and

$$\frac{\delta\rho}{\rho} = \frac{\delta(\Gamma_1 p)}{\Gamma_1 p} - \frac{\delta c^2}{c^2} . \qquad (A13)$$

Now an interval $[\tau_a, \tau_b]$ is considered, with $0 < \tau_a < \tau_b < \tau_t$ and $\tau_b - \tau_a \ll \tau_t$, such that $\delta c^2/c^2$, $\delta(\Gamma_1 p)/\Gamma_1 p$ and all their derivatives are equal to zero outside it. Integrating Eq. (A7) by parts we obtain

$$\delta I = \int_{\tau_a}^{\tau_b}\left[\frac{\mathrm{d}^2\delta B_1}{\mathrm{d}\tau^2}\overline{\overline{E_r^2}} + \frac{\mathrm{d}^2}{\mathrm{d}\tau^2}(\delta B_2 + \delta B_0)\,\overline{E_r^2} + \frac{\mathrm{d}^2\delta B_3}{\mathrm{d}\tau^2}E_r^2\right]\mathrm{d}\tau , \qquad (A14)$$

with

$$\overline{\overline{E_r^2}}(\tau) = \int^{\tau} \overline{E_r^2}(\tau_1)\,\mathrm{d}\tau_1 = \int^{\tau} \left[\int^{\tau_1} E_r^2(\tau_2)\,\mathrm{d}\tau_2\right] \mathrm{d}\tau_1 \,. \qquad (A15)$$

We have asymptotically that in this region

$$E_r(\tau) \sim E_0 \cos\left[\omega \int_0^{\tau} \left(1-\frac{S_l^2}{\omega^2}\right)^{1/2} \mathrm{d}\tau + \phi\right] \sim E_0 \cos(\Lambda/2)\,, \qquad (A16)$$

where E_0 is the amplitude of the eigenfunction envelope, and we use $\Lambda(\tau)$ to represent twice the argument of the eigenfunction. It then follows that

$$\overline{\overline{E_r^2}} \sim \frac{1}{2} E_0^2 \left[\frac{\tau^2+2e_1\tau+2e_2}{2} - \frac{\cos(\Lambda)}{4\omega^2(1-\Delta)}\right] , \qquad (A17)$$

where the e_i's are constants of integration.

It follows from the equation of hydrostatic support that any discontinuity in the m^{th} derivative of c^2 is associated with a discontinuity in the $(m+1)^{th}$ derivative of $\Gamma_1 p$ (provided that discontinuities in Γ_1 arising from the change in thermodynamic state can be ignored). Hence we shall neglect the contributions from the terms in $\delta(\Gamma_1 p)$, being left with only terms in the integral which are coefficients of $\delta c^2/c^2$ or its derivatives.

If the n^{th} derivative of the sound speed in the original structure of the star is discontinuous we have that

$$\frac{\mathrm{d}^{n+1}}{\mathrm{d}\tau^{n+1}}\left[h_j(\tau)\frac{\delta c^2}{c^2}\right] \sim A_{\delta k}\, h_j(\tau)\, \delta(\tau-\tau_d)\,, \qquad (A18)$$

where τ_d is the acoustic depth of the discontinuity, $A_{\delta k}$ the amplitude associated with the δ-function and h_j any of the coefficients of $\delta c^2/c^2$ in Eqs (A8) – (A11) which are slowly varying functions of τ. We label the cases without and with overshoot with index k = 1 and 2, respectively.

Consider first the case with overshoot. Here the delta function appears in the second derivative of c, and hence Eq. (A14) is already of the appropriate form. Substituting Eq. (A18) into Eq. (A14) we obtain a periodic component δI_p of the form

$$\delta I_{p2} \sim D_2(\omega,l,r_d)\cos\left[2\omega\int_0^{\tau_d}\left(1-\frac{S_l^2}{\omega^2}\right)^{1/2}\mathrm{d}\tau + 2\phi\right] . \qquad (A19)$$

For most of the modes considered $\Delta \ll 1$ at the discontinuity; this condition corresponds to requiring that the lower turning points of the modes are substantially deeper than the location of the discontinuity. Furthermore, we note that for the high-order acoustic modes considered $\omega \gg (g/r)^{1/2} \sim (g_s/R)^{1/2}$, g_s being the surface gravity of the star. From Eqs (A8) – (A11) we then have that

$$\begin{aligned} \delta B_0 + \delta B_2 &\sim \mathscr{O}(\omega^0)\,, \\ \delta B_1 &\sim \mathscr{O}(\omega^2)\,, \\ \delta B_3 &\sim \mathscr{O}(\omega^0)\,. \end{aligned} \qquad (A20)$$

Furthermore,

$$E_r^2 \,/\, \overline{E_r^2} \sim \mathscr{O}(\omega^1)\,, \qquad E_r^2 \,/\, \overline{\overline{E_r^2}} \sim \mathscr{O}(\omega^2)\,, \qquad (A21)$$

so that the dominant contributions (i.e., those with the highest power in ω) are the factors associated with δB_1 and δB_3. Thus

$$D_2(\omega,l,r_d) \sim \left[\frac{1}{8\omega^2}\frac{\omega^2}{(1-\Delta)^2} - \frac{1}{4}\frac{\Delta}{(1-\Delta)^2}\right] A_{\delta 2}\, E_0^2 \sim \frac{A_{\delta 2}}{8}\frac{1-2\Delta}{(1-\Delta)^2}\, E_0^2\,. \qquad (A22)$$

Note that for small S_l/ω the Δ-dependence in this expression is $\mathscr{O}(\Delta^2)$, and so the amplitude D_2 depends only weakly on the degree.

In the case without overshoot, the second derivative is discontinuous rather than the first; to obtain a delta function, we therefore integrate Eq. (A14) once again to obtain

$$\delta I = \int_{\tau_a}^{\tau_b}\left[\frac{\mathrm{d}^3\delta B_1}{\mathrm{d}\tau^3}\,\overline{\overline{\overline{E_r^2}}} + \frac{\mathrm{d}^3}{\mathrm{d}\tau^3}(\delta B_2+\delta B_0)\,\overline{\overline{E_r^2}} + \frac{\mathrm{d}^3\delta B_3}{\mathrm{d}\tau^3}\,\overline{E_r^2}\right]\mathrm{d}\tau\,, \qquad (A23)$$

where

$$\overline{\overline{\overline{E_r^2}}}(\tau) = \int^{\tau}\overline{\overline{E_r^2}}(\tau_1)\,\mathrm{d}\tau_1 \sim \frac{1}{2}E_0^2\left[\frac{\tau^3+3e_1\tau^2+6e_2\tau+3e_3}{6} - \frac{\cos(\Lambda)}{8\omega^3(1-\Delta)^{3/2}}\right] . \qquad (A24)$$

Hence in this case we obtain

$$\delta I_{p1} \sim D_1(\omega,l,r_d)\,\sin\left[2\omega\int_0^{\tau_d}\left(1-\frac{S_l^2}{\omega^2}\right)^{1/2}\mathrm{d}\tau + 2\phi\right] , \qquad (A25)$$

where the dominant contribution is

$$D_1(\omega,l,r_d) \sim \frac{A_{\delta 1}}{16\omega}\frac{1-2\Delta}{(1-\Delta)^{5/2}}\, E_0^2\,. \qquad (A26)$$

Finally, from in Eq. (5) we get

$$I_1 \simeq \int_0^{\tau_t} E_r^2 \mathrm{d}\tau \sim \frac{1}{2}\tau_t E_0^2\,. \qquad (A27)$$

Hence in both cases, without and with overshoot, we can write the oscillatory component of the frequency as (omitting the dependence of the amplitudes $A_k = D_k/\tau_t\omega E_0^2$ on r_d)

$$\delta\omega_{pk} = \frac{\delta I_{pk}}{2\omega I_1} \sim A_k(\omega,l)\cos\left[2\omega\int_0^{\tau_d}\left(1-\frac{S_l^2}{\omega^2}\right)^{1/2}\mathrm{d}\tau + 2\phi_k\right] . \qquad (A28)$$

Thus it follows from Eqs (A19), (A22), (A25) and (A26) that $A_2/A_1 \propto \omega$ and $\phi_1 - \phi_2 \sim \pi/4$. To cover both cases, we express the amplitude as

$$A(\omega, l) \sim \frac{1-2\Delta}{(1-\Delta)^2}\left[\frac{a_1}{(1-\Delta)^{1/2}}\left(\frac{\tilde{\omega}}{\omega}\right)^2 + a_2\left(\frac{\tilde{\omega}}{\omega}\right)\right], \quad (A29)$$

where $\tilde{\omega}$ is chosen to correspond to a cyclic frequency of 2500 μHz and a_1 and a_2 are two constants associated with the structure at the discontinuity. It follows from our asymptotic considerations that we expect $a_2 \ll a_1$ if overshoot is not present and $a_1 \ll a_2$ if it is.

Note that for small values of S_l/ω the factor in Δ is $\mathcal{O}(\Delta^2) = \mathcal{O}(S_l^4/\omega^4)$ while the one associated with a_1 is approximately $1 + S_l^2/2\omega^2 \sim 1 + \mathcal{O}(\Delta)$. Therefore the amplitude can be considered weakly dependent on degree.

Appendix B: simple example

We consider the following equation:

$$\frac{d^2Y}{d\tau^2} + [\omega^2 - V^2(\tau)]Y(\tau) = 0\,, \quad (B1)$$

and determine the eigenfunction $Y(\tau)$ which is the solution for the eigenvalue ω for a given potential $V(\tau)$. As boundary conditions we take reflecting boundaries ($Y=0$) at $\tau=0$ and $\tau=\tau_t$.

Our reference solution is assumed to correspond to the potential being constant everywhere, $V=V_a$, say. The solution for frequency ω_0, satisfying the boundary condition at $\tau = 0$, is

$$Y(\tau) = A_0 \sin\left[\int_0^\tau (\omega_0^2 - V_a^2)^{1/2}\, d\tau\right], \quad (B2)$$

where A_0 is a constant. Imposing also the boundary condition at $\tau = \tau_t$, we obtain the following dispersion relation:

$$\omega_0^2 - V_a^2 = \left(\frac{n\pi}{\tau_t}\right)^2, \quad (B3)$$

n being an integer corresponding to the (*number of zeros* -1) of the eigenfunction.

To illustrate the effects of discontinuities or singularities, we consider two perturbed potentials. The first is defined by

$$V_1(\tau) = \begin{cases} V_b & \text{for } 0 \le \tau < \alpha_1\tau \\ V_a & \text{for } \alpha_1\tau \le \tau < \tau_t\,, \end{cases} \quad (B4)$$

while the second is given by

$$V_2(\tau) = V_a + A_\delta \delta(\tau - \alpha_2\tau_t) \quad (B5)$$

(see also Fig. 2). Imposing the same boundary conditions, and requiring that $Y(\tau)$ be continuous everywhere, we find the solutions for the two cases as, respectively,

$$\begin{cases} Y_{11}(\tau) = A_1 \dfrac{\sin[\Lambda_b(\tau)]}{\sin[\Lambda_b(\alpha_1\tau_t)]} & \text{for } 0 \le \tau \le \alpha_1\tau_t \\ Y_{12}(\tau) = A_1 \dfrac{\sin[\Lambda_a(\tau_t - \tau)]}{\sin[\Lambda_a(\tau_t - \alpha_1\tau_t)]} & \text{for } \alpha_1\tau_t \le \tau \le \tau_t \end{cases} \quad (B6)$$

and,

$$\begin{cases} Y_{21}(\tau) = A_2 \dfrac{\sin[\Lambda_a(\tau)]}{\sin[\Lambda_a(\alpha_2\tau_t)]} & \text{for } 0 \le \tau \le \alpha_2\tau_t \\ Y_{22}(\tau) = A_2 \dfrac{\sin[\Lambda_a(\tau_t - \tau)]}{\sin[\Lambda_a(\tau_t - \alpha_2\tau_t)]} & \text{for } \alpha_2\tau_t \le \tau \le \tau_t\,. \end{cases} \quad (B7)$$

Here A_1 and A_2 are constants, and

$$\Lambda_j(\tau) = \int_0^\tau (\omega^2 - V_j^2)^{1/2} d\tau = (\omega^2 - V_j^2)^{1/2}\tau\,;\ j = a, b\,. \quad (B8)$$

We now need to impose a condition on $dY/d\tau$. To do so, Eq. (B1) is integrated around $\alpha_i\tau_t$ ($i=1,2$), giving

$$\int_{\alpha_i\tau_t - \epsilon}^{\alpha_i\tau_t + \epsilon} \frac{d^2Y}{d\tau^2} d\tau = -\int_{\alpha_i\tau_t - \epsilon}^{\alpha_i\tau_t + \epsilon} (\omega^2 - V^2)\, Y d\tau\,. \quad (B9)$$

Substituting the potentials in Eqs (B4) and (B5), and taking the limit $\epsilon \to 0$ of these relations, we obtain the matching conditions

$$\left[\frac{dY_{12}}{d\tau} - \frac{dY_{11}}{d\tau}\right]_{\alpha_1\tau_t} = 0\,, \quad (B10)$$

and

$$\left[\frac{dY_{22}}{d\tau} - \frac{dY_{21}}{d\tau}\right]_{\alpha_2\tau_t} = A_\delta\, Y_{21}(\alpha_2\tau_t) = A_\delta\, Y_{22}(\alpha_2\tau_t)\,, \quad (B11)$$

in the two cases. By using the solutions given in Eqs (B6) and (B7), we finally derive the following two dispersion relations:

$$\tan[\Lambda_b(\alpha_1\tau_t)] = -\left(\frac{\omega^2 - V_b^2}{\omega^2 - V_a^2}\right)^{1/2} \tan[\Lambda_a(\tau_t - \alpha_1\tau_t)] \quad (B12)$$

and

$$\tan[\Lambda_a(\alpha_2\tau_t)] = -\frac{\tan[\Lambda_a(\tau_t - \alpha_2\tau_t)]}{1 - A_\delta(\omega^2 - V_a^2)^{-1/2}\tan[\Lambda_a(\tau_t - \alpha_2\tau_t)]}\,. \quad (B13)$$

These relations determine the values of ω satisfying the boundary conditions for the first case in terms of V_a, V_b and α_1, while in the second case in terms of V_a, A_δ and α_2.

We now expand the expressions to first order in the small quantities $\delta\omega = \omega - \omega_0$, $\delta V^2 = V_a^2 - V_b^2$ and V_i^2/ω^2. For the step-function potential $V_1(\tau)$ we obtain the periodic component of $\delta\omega$, given by

$$\delta\omega_{p1} \sim \frac{\delta V^2}{4\tau_t\omega_0^2} \sin[2\Lambda_0(\alpha_1\tau_t)]\,, \quad (B14)$$

while the delta-function potential $V_2(\tau)$ gives rise to a periodic component

$$\delta\omega_{p2} \sim \frac{A_\delta}{2\tau_t\omega_0} \cos[2\Lambda_0(\alpha_2\tau_t)]\,; \quad (B15)$$

here

$$\Lambda_0(\tau) = \int_0^\tau (\omega_0^2 - V_a^2)^{1/2} d\tau\,. \quad (B16)$$

Appendix C: numerical method

In this Appendix we describe in detail the numerical procedure used in the process of isolating the oscillatory signal associated with a discontinuity, as discussed in Sect. 4.

The principle of the method is to subtract from the frequencies ω_{nl} a smoothed frequency $\omega_{nl}^{(s)}$, and to fit the residual to the periodic signal $\delta\omega_p$ in Eq. (20), with $A(\omega)$ represented by Eq. (12). Thus we have developed a process that will iterate to determine the minimum of

$$\mathscr{R} = \sum_l \left\{ \sum_n \left[(\omega_{nl} - \omega_{nl}^{(s)}) - f(\omega_{nl}) \right]^2 \right\} . \qquad (C1)$$

Here the function $f(\omega_{nl})$ is expressed as

$$f(\omega_{nl}) = \left[a_1 \left(\frac{\tilde{\omega}}{\omega_{nl}} \right)^2 + a_2 \left(\frac{\tilde{\omega}}{\omega_{nl}} \right) \right] \times \cos\left(2\omega_{nl}\overline{\tau}_d - \overline{\gamma}_d \frac{L^2}{\omega_{nl}} + 2\phi_0 \right) , \qquad (C2)$$

with $\tilde{\omega}/2\pi = 2500\,\mu$Hz.

The smooth frequency $\omega_{nl}^{(s)}$ is obtained separately for each degree l, fitting a smoothing function of mode order n, to the reduced frequency

$$\omega_{nl}^{(r)} = \omega_{nl} - f(\omega_{nl}) . \qquad (C3)$$

As smoothing functions use the polynomials

$$p_l(n) = \sum_{k=1}^{N_l} a_k^{(l)}\, n^{k-1} , \qquad (C4)$$

constructed for each l, given the N_l points $(n, \omega_{nl}^{(r)})$, by determining the values a_k $(k=1, \ldots, N_l)$ that minimize

$$\sum_{i=1}^{N_l} \left\{ \left[p_l(n_i) - \omega_{n_i l}^{(r)} \right]^2 + \lambda \left(\frac{\mathrm{d}^3 p_l}{\mathrm{d}n^3} \right)_{n_i}^2 \right\} . \qquad (C5)$$

If $\lambda = 0$, p_l will interpolate all points; however for non-zero λ the second term will try to reduce the third derivative of p_l, making it smoother. The choice of a smoothing condition based on derivatives of frequency comes from the fact that components varying over a shorter scale in frequency dominate in higher derivatives. Therefore, we have selected the lowest derivative of $\omega(n)$ for which the signal from the base of the convection zone dominates over the signal from the helium ionization zone, and at the same time the smooth component of the frequencies is removed.

The actual numerical procedure consists of finding the parameters $a_1, a_2, \overline{\tau}_d, \overline{\gamma}_d$ and ϕ_0 minimizing $\mathscr{R}$ using two iterative cycles. The inner cycle iterates, given a value of λ, the values of the parameters in $f(\omega_{nl})$ in order to decrease $\mathscr{R}$; thus, using the same λ we repeat the cycle:

$$\text{find } \omega_{nl}^{(r)} \rightarrow \text{smooth } \omega_{nl}^{(r)} \rightarrow \text{fit } (\omega_{nl} - \omega_{nl}^{(s)}) \text{ by } f(\omega_{nl}).$$

This iteration is surrounded by an outer cycle, where λ is successively reduced by a factor two. In the initial step of these cycles we take $f(\omega_{nl}) \equiv 0$ when determining $\omega_{nl}^{(r)}$, since in this step all parameters are unknown.

This group of steps will isolate from ω_{nl} a component of the form given by Eq. (20), returning the best values of the parameters, in a least-squares sense, characterizing the signal. The initial value λ_0 of λ determines the period of the signal to be isolated. If λ_0 is chosen to be larger, the smoothing step fails to remove the signal associated with the helium ionization zone, which would then dominate the least-squares fit (C1). Here we have used the same $\lambda_0, 4\times10^{-7}$, in all fits to model and observed frequencies.

Note that the observational uncertainties σ_{nl} have not been included in the expressions (C1) and (C5). Because σ_{nl} increases with ω or n (see the error bars in Fig. 9), taking the uncertainties into account in the least-squares fits would give relatively more weight to low-frequency data, where the signal from the helium ionization zone has a larger amplitude. The result would be a systematic error in the inferred value of $\overline{\tau}_d$ due to the contamination of the smooth function from such a signal, as well as of the fitting. One can of course take the uncertainties on individual mode frequencies into account while introducing an extra weighting to compensate for the general trend of the uncertainties with frequency, but we have chosen not to do so, given the arbitrariness of such a weighting.

References

Alongi M., Bertelli G., Bressans A., Chiosi C., 1991, A&A 244, 95

Basu S., Antia H. M., Narasimha D., 1993, MNRAS in press.

Berthomieu G., Morel P., Provost J, Zahn J.-P., 1993, in: Inside the Stars, eds. A. Baglin and W. W. Weiss, PASPC 40, 60

Chandrasekhar S., 1964, ApJ 139, 664

Christensen-Dalsgaard J., 1982, MNRAS 199, 735

Christensen-Dalsgaard J., Pérez Hernández F., 1991, in: Challenges to theories of the structure of moderate-mass stars, Lecture Notes in Physics, vol. 388, eds D. O. Gough, J. Toomre, Springer, Heidelberg, p. 43

Christensen-Dalsgaard J., Pérez Hernández F., 1992, MNRAS 257, 62

Christensen-Dalsgaard J., Thompson M. J., 1991, ApJ 367, 666

Christensen-Dalsgaard J., Gough D. O., Thompson M. J., 1989, MNRAS 238, 481

Christensen-Dalsgaard J., Gough D. O., Thompson M. J., 1991, ApJ 378, 413

Gough D. O., 1990, in: Progress of Seismology of the Sun and Stars, eds. Y. Osaki and H. Shibahashi, Lecture Notes in Physics 367, Springer-Verlag, p. 283

Gough D. O., Sekii T., 1993, in Seismic Investigation of the Sun and Other Stars, ed. T. M. Brown, PASPC 42, 177.

Gough D. O., Vorontsov S., 1993, MNRAS (submitted)

Libbrecht K. G., Wodard M. F., Kaufman J. M., 1990, ApJS 74, 1129

Maeder A., 1976, A&A 47, 389

Monteiro M. J. P. F. G., Christensen-Dalsgaard J., Thompson M. J., 1993a, in: Inside the Stars, eds. A. Baglin and W. W. Weiss, PASPC 40, 557

Monteiro M. J. P. F. G., Christensen-Dalsgaard J., Thompson M. J., 1993b, in: Seismic Investigation of the Sun and Other Stars, ed. T. M. Brown, PASPC 42, 253.

Pidatella R. M., Stix M., 1986, A&A 157, 338

Roxburgh I. W., Vorontsov S. V., 1993, in: Seismic Investigation of the Sun and Other Stars, ed. T. Brown, PASPC 42, 169.

Schmitt J. H. M. M., Rosner R., Bohn H. U., 1984, ApJ 282, 316

Thompson M. J., 1988, in: Seismology of the Sun and Sun-like Stars, ed. E. J. Rolfe, ESA SP-286, ESTEC, Noordwijk, p. 321

Unno W., Osaki Y., Ando H., Shibahashi H., 1979, Nonradial Oscillations of Stars, University of Tokyo Press

Vorontsov S., 1988, in: Proc. IAU Symposium No 123, Advances in Helios- and Asteroseismology, eds. J. Christensen-Dalsgaard and S. Frandsen, Reidel, p. 151

Vorontsov S. V., Zharkov V. N., 1989, Sov. Sci. Rev. E. Astrophys. Space Phys. 7,1

Vorontsov S. V., Baturin V. A., Pamyatnykh A. A., 1991, Nat 349, 49

Vorontsov S. V., Baturin V. A., Pamyatnykh A. A., 1992, MNRAS 257, 32

Zahn J.-P., 1991, A&A 252, 179

This article was processed by the author using Springer-Verlag TEX A&A macro package 1992.